NANO LETTERS

2008
Vol. 8, No. 8
2510-2516

Ab Initio Study of Phonon-Induced Dephasing of Electronic Excitations in Narrow Graphene Nanoribbons

Bradley F. Habenicht,[†] Oleg N. Kalugin,[‡] and Oleg V. Prezhdo*,[†]

Department of Chemistry, University of Washington, Seattle, Washington 98195-1700, USA and Department of Chemistry, Kharkiv National University, Kharkiv, 61007, Ukraine

Received May 31, 2008; Revised Manuscript Received June 30, 2008

ABSTRACT

Vibrational dephasing of the lowest energy electronic excitations in the perfect (16,16) graphene nanoribbon (GNR) and those with the C_2-bond insertion and rotation defects is studied with ab initio molecular dynamics. Compared to single-walled carbon nanotubes (SWCNTs) of similar size, GNRs shows very different properties. The dephasing in the ideal GNR occurs twice faster than that in the SWCNTs. It is induced primarily by the 1300 cm^{-1} disorder mode seen in bulk graphite rather than by the 1600 cm^{-1} C−C stretching mode as in SWCNTs. In contrast to SWCNTs, defects exhibit weaker electron−phonon coupling compared to the ideal system. Therefore, defects should present much less of a practical problem in GNRs compared to SWCNTs. The predicted optical line widths can be tested experimentally.

The past two decades have seen a revival in scientific research on carbon-based materials. The primary reason for this renaissance is the identification and emergence of several nanostructured allotropes of carbon. Fullerenes appeared in 1985[1] and were shortly followed in 1991 with carbon nanotubes,[2] which have been heavily studied ever since. A new discovery came in 2004 with the isolation of single sheets of graphite, or graphene, by mechanical exfoliation.[3] This carbon nanostructure, once thought unstable, has once again captured the imagination of the scientific community, and interest in this new form of carbon has already received a great amount of attention. Synthesis methodologies have vastly improved in the past few years from isolation with tape to chemical vapor deposition[4] and, recently, solution processing.[5] The enhanced ability to isolate single, quasi-two-dimensional graphene sheets has provoked a detailed undertaking of the study of its intrinsic properties.

Perhaps the greatest driving force for the study of graphene is its potential to replace the channel material in field effect transistors (FETs).[6] Single-walled carbon nanotubes (SWCNTs) were once expected to hold this honor;[7] however the mixture of semiconducting and metallic SWCNTs produced during synthesis is a major roadblock. Although large graphene sheets are zero band gap semimetals, it has been shown theoretically[8–10] and experimentally[11–13] that quantum confinement effects in narrow graphene nanoribbons (GNR) cause an opening of the band gap. This important verification allows for the patterning of GNRs in FETs without the difficulties associated with SWCNTs. Further, it was recently demonstrated that GNR FETs may be etched lithographically to a size of less than 10 nm.[11] This is an important landmark, since current Si-based FETs are built using lithographic techniques. As GNRs are envisioned as an electronic material of the future, a detailed knowledge of their fundamental properties is of the utmost importance.

The electron−phonon interaction influences the electron mean-free-path in nanoribbon FETs and, therefore, determines the length of the FET channel as well as the switching speed of the device.[6] The electron−phonon interaction and phonon-induced electronic dephasing can be expected to play important roles in many other potential applications of GNRs. Charge-phonon scattering will be the main source of energy dissipation and loss in future GNRs electronic devices. Phonon-induced electronic dephasing sets coherence limits on spin[14,15] and charge transport.[16] Electron−phonon interactions can create distortions in GNR geometric structure and, therefore, affect many of their mechanical and electronic properties.

The present Letter reports the first ab initio study of the vibrationally induced pure-dephasing of the lowest energy electronic excitations in narrow GNRs. Using ab initio molecular dynamics (MD), for the first time, we compute pure-dephasing times in a perfect GNR and the same GNR with two typical defects. Surprisingly, we find that compared to SWCNTs of similar size, GNRs show very different

* Corresponding author, prezhdo@u.washington.edu.
[†] University of Washington.
[‡] Kharkiv National University.

10.1021/nl801556n CCC: $40.75
Published on Web 07/23/2008

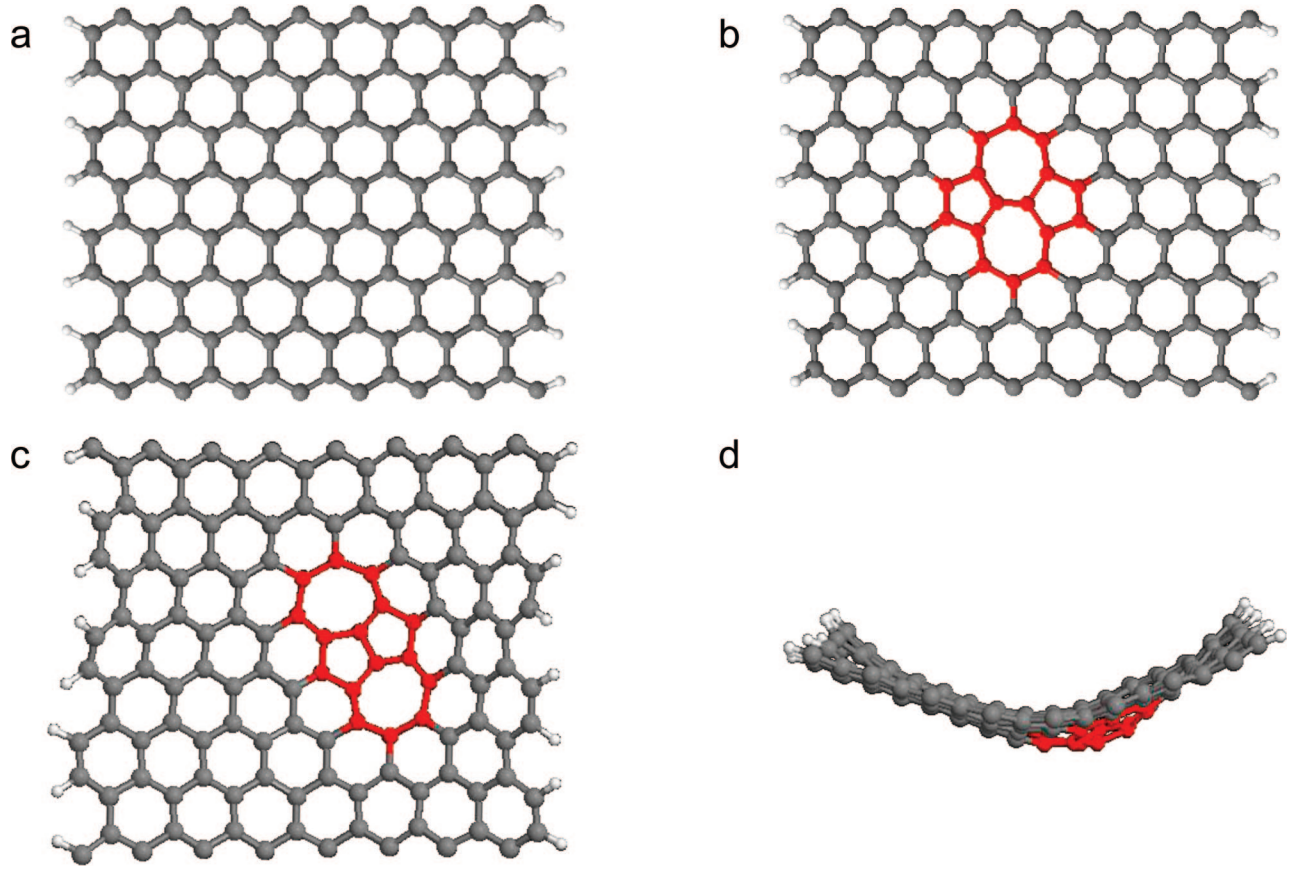

Figure 1. Geometric structure of (a) ideal (16,16) GNR and (16,16) GNR with (b) SW and (c) 7557 defects. Carbon atoms that are part of the five- and seven-member rings of the defects are depicted in red. The distortion of the ribbon caused by the 7557 defect is illustrated in part (d).

dephasing features. Even though dephasing in the ideal GNR is induced by slower modes than in SWCNTs, it occurs about twice as fast. The defects create significant distortions in the GNR structure and localized electronic excitations. Unexpectedly, the electron−phonon interactions created by the defects are weaker than those in the ideal GNR, which is in contrast to SWCNTs. This result has particularly important practical consequences, because many of the electronics applications of SWCNTs are limited by defects, which efficiently dissipate the excitation energy and quench fluorescence.

Since defects reduce the electron−phonon interaction in the current case, similar practical problems should not arise in GNRs.

The vibrational dephasing of electronic excitations can be probed directly by time-resolved laser experiments, such as photon-echo. Alternatively, it can be determined experimentally by the absorption or emission line widths detected using energy-domain spectroscopies, such as photoluminescence.[17] At present, these data for graphene sheets are not yet available in the literature. In analog to SWCNTs, which have fluoresced from many environments,[18–20] it can be expected that advances in synthesis will allow photoluminescence studies on GNRs. Possible strategies may involve the growth of GNRs across nanostructures[21] or the etching away of substrate to eliminate extraneous nonradiative decay channels.[22] The recent report of the solution phase synthesis and stabilization of narrow GNRs[5] provides another plausible candidate for the optical studies.

The current simulation uses the (16,16) armchair GNR with a width of 1.8 nm. The dangling bonds on the edges of the GNR are terminated with hydrogens, Figure 1. The Stone-Wales (SW) and 7557 defects chosen here are well-known for SWCNTs[23] and represent the same disruption in the perfect hexagonal periodicity of graphene, obtained by different means. The SW defect is a rotation of a C−C dimer in the plane of the GNR. The 7557 defect involves insertion of a C−C dimer and leads to a much larger distortion in both the electronic and geometric structure. While the GNR with the SW defect remained relatively flat during the simulation, the 7557 caused a large buckling of the ribbon (Figure 1d). The SW and 7557 changes in the bonding pattern are relatively minor, since they do not involve dangling bonds or heteroatoms, though they have been shown to affect the reactivity of SWCNTs.[24] Generally, one can expect that changes in the GNR properties will be similar but more pronounced with more major defects.

The molecular dynamics (MD) simulations were performed using the Vienna Ab Initio Simulations Package.[25] The Perdew−Wang generalized gradient approximation[26] with projector-augmented-wave pseudopotentials[27,28] was employed in a converged plane-wave basis. Periodic boundary conditions were used along the length of the GNRs and five unit cells were incorporated in order to expand the

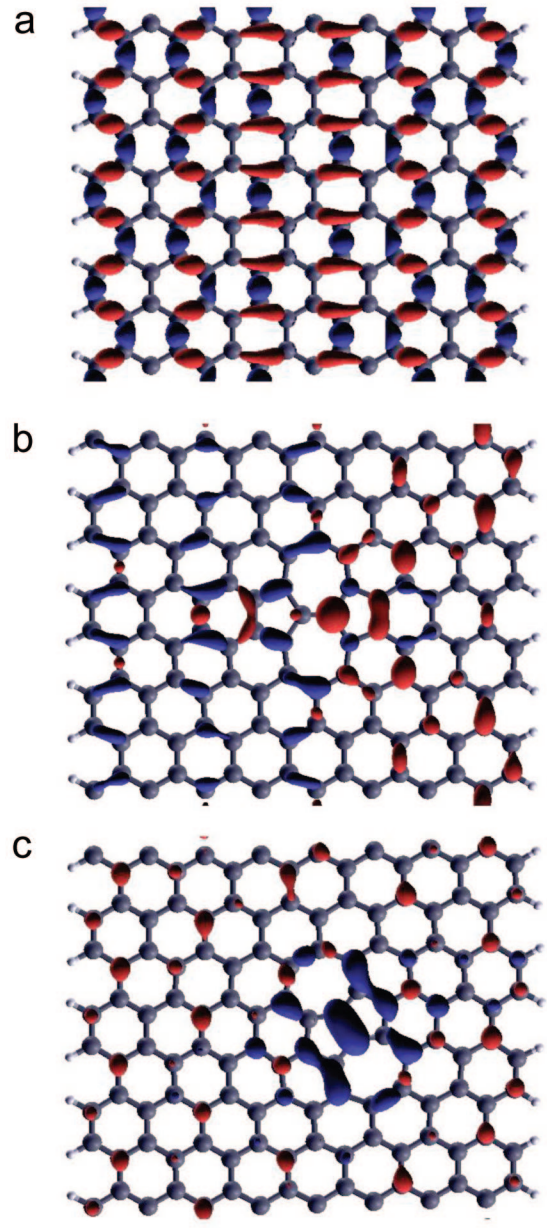

Figure 2. Transition densities of the lowest energy excitations in (a) ideal (16,16) GNR, (b) (16,16) GNR with the SW defect, and (c) (16,16) GNR with the 7557 defect. Red and blue correspond to positive and negative density changes.

phonon spectrum. Eight angstroms of vacuum were used in the directions perpendicular to the length of the ribbon in order to avoid spurious interactions. All ribbons were relaxed to their minimum-energy geometries and then heated to 300 K via repeated velocity rescaling. Trajectories were obtained using the Verlet integration algorithm and Hellmann−Feynman forces in the microcanonical ensemble. Distortion of the two-dimensional (2D) lattice due to the 7557 defect was not observed during the energy minimization and only occurred during the MD run, indicating that defect relaxation involves an energy barrier. The data involving the defect relaxation were removed from the analysis.

Figure 2 shows the transition density for the lowest energy excitation in the perfect (16,16) GNR as well as the disruption of the excitation density caused by the defects. Both defects localize the transition density. The localization is more pronounced with the 7557 C−C bond insertion. The calculated excitation energy of 0.72 eV for the ideal (16,16) GNR agrees well with a recent study on small width GNRs.[8] As should be expected with pure DFT functionals the excitation energy is smaller than that obtain from the hybrid HSE exchange-correlation functional[8] and many-body perturbation theory within the GW approximation.[9] However, the HSE and GW approaches are much more computationally demanding than the present scheme and cannot be used in our time-domain simulation. Both methods show that the simpler methodology is qualitatively correct in predicting the excitation energy. Further, the dephasing function depends only on the relative fluctuations of the energy and not its absolute magnitude. The SW defect slightly lowered the excitation energy to 0.68 eV, while the 7557 defect created a new state at 0.62 eV. Experimental data show that electronic excitations in graphene relax on ultrafast time scales.[29,30] Therefore, we assume, similarly to CNTs,[31,32] that in narrow semiconducting GNRs higher energy excitations relax rapidly to the lowest excited state and focus on fluorescence line widths and dephasing times associated with this state.

The theory of optical absorption and emission line-shapes is well-established.[17,33] The width of the observed optical bands can be split into two components. Inhomogeneous broadening occurs due to different local conditions of each species in the ensemble, while homogeneous broadening is determined by the lifetime of the excited state T_1 and the pure-dephasing time T_2^*. In the absence of inhomogeneous broadening, which can be eliminated by photon-echo or single molecule experiments, the line width Γ may be expressed as

$$\Gamma = \frac{1}{T_2} = \frac{1}{2T_1} + \frac{1}{T_2^*} \tag{1}$$

As is well established for semiconducting SWCNTs, which should be similar to graphene sheets, the lifetime is significantly longer than the pure-dephasing time, and the line width is determined by the latter quantity.

The autocorrelation function (ACF) of the excited-state energy

$$C(t) = \langle \Delta E(t) \Delta E(0) \rangle_T \tag{2}$$

provides direct information regarding the phonon-induced fluctuation of the electronic energy and can be used in order to obtain the pure-dephasing function. $\langle \cdots \rangle_T$ denotes canonical averaging. The ACF is unnormalized, and its initial value represents the average fluctuation of the excitation energy. Figure 3 compares the ACFs of the ideal (16,16) GNR with those of the defects. The dephasing time scales depend not only on the decay rate of the ACF but also on its initial value. The ACFs of the defects decay on a 100 fs time scale, much more quickly than the ACF of the ideal ribbon. Although the ACF of the ideal GNR oscillates coherently for a long time, suggesting that the dephasing might be slow, the magnitude of the oscillation is larger than that of the defects. The calculation below shows that the large magnitude oscillation of the ACF for the ideal ribbon is responsible for faster dephasing relative to the defects.

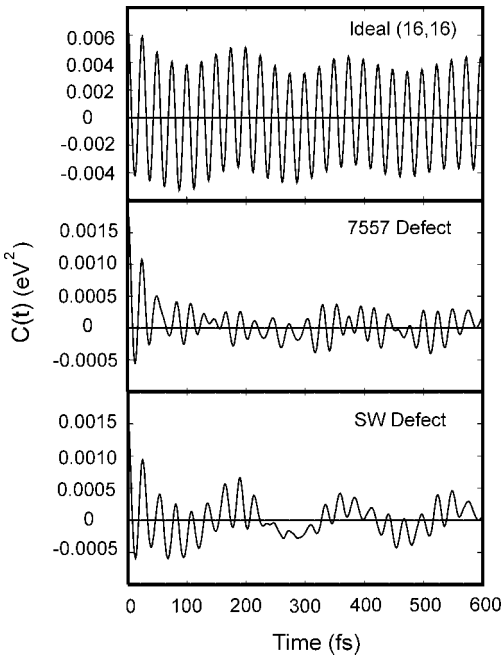

Figure 3. Autocorrelation functions (ACF) of the lowest excitation energy, eq 4, for the GNRs under investigation. The average fluctuation of the excitation energy provided by the initial value of the ACF is significantly smaller in the case of defects. The energy fluctuation is also more random with defects, resulting in a faster decay of the ACF.

The Fourier transform (FT) of the ACFs establishes the phonon modes that are responsible for the dephasing, Figure 4. The ideal ribbon couples strongly to the phonon mode at 1345 cm^{-1}. This mode was identified as a disorder mode and was recently detected at the edges of single graphene sheets by Raman spectroscopy.[34] The narrow width of the ribbon emphasizes the importance of the edges. In contrast, SWCNTs couple most strongly to the C−C stretch at a frequency close to 1600 cm^{-1}.[35,36] The defects couple to a wide range of modes, although much more weakly. Note that in Figure 4 the spectral density of the two defects has been multiplied by 20 for comparison with the ideal ribbon. The weaker coupling of the defect states to the phonon modes is surprising and counterintuitive at first, since in general, and in CNTs in particular,[37,38] localized electronic excitations generate larger perturbations in the atomic lattice and, therefore, stronger electron−phonon coupling. The explanation resides in the lack of stiffness of the ribbons compared to the tubes. Defects per se behave similarly in the two carbon materials. In fact, the dephasing induced by the SW defect is almost identical in the GNR and SWCNTs.[37] The 7557 defect shows different properties in GNRs and SWCNTs, because it is able to relax and substantially distort the ribbon, Figure 1d. The corresponding relaxation of the defect is not possible in the much more rigid SWCNTs. Ribbons may be regarded as an intermediate between SWCNTs exhibiting weaker electron−phonon coupling[38,39] and conjugated polymers showing stronger coupling.[40,41]

An estimate of the dephasing time may be calculated using the second-order cumulant expansion, which gives a perturbative description of the optical response function.[17] The term that is linear with respect to ΔE vanishes upon canonical averaging. The ACF represents the second-order approximation. It is doubly integrated and exponentiated, producing the dephasing function

$$D_c(t) = e^{-g(t)} \tag{3}$$

where

$$g(t) = \int_0^t d\tau_1 \int_0^t C(\tau_2)\, d\tau_2$$

The dephasing function can also be obtained directly, avoiding the cumulant expansion, but requiring averaging over an oscillatory exponential function

$$D(t) = \exp[i\langle \Delta E\rangle_T t/\hbar]\left\langle \exp\left\{-\frac{i}{\hbar}\int_0^t \Delta E(\tau)\, d\tau\right\}\right\rangle_T \tag{4}$$

The cumulant approximation converges faster than the direct calculation.

The dephasing functions calculated using the direct method are shown in Figure 5. The plots for the ideal GNR and the GNRs with the defects are qualitatively different and were fit with two separate equations in order to extract the dephasing time scales. The dephasing function of the ideal ribbon was fit using

$$f_A(t) = \exp(-t/\tau)\frac{1 + A\cos(\omega t)}{1 + A} \tag{5}$$

where ω is the frequency of the oscillations seen on top of the decay. The GNRs with defects showed little oscillations but required a Gaussian component in order to obtain a good fit

$$f_B(t) = [B\exp(-t/\tau_e) + (1 - B)\exp(-t/\tau_g)^2] \tag{6}$$

Here, B gives the magnitude of the exponential decay component. The fitting results are shown in Table 1. The frequency ω obtained from the ACF fit (5) corresponds to the 1345 cm^{-1} phonon mode observed in the FT data shown in Figure 4. It should be noted that the dephasing fits were truncated at 100 fs, even though the ACF of the ideal GNR shows a longer, picosecond decay component, Figure 3. Following a rapid decay to zero, $D(t)$ for the ideal GNR exhibits recurrences, occasionally returning to approximately 20% of its initial value. We are unable to investigate this long-time decay component due to computational expense. We believe that in experiments interactions with the environment will dampen this long time decay component of the dephasing function. The optical line width is inversely proportional to the dephasing time, and therefore, the shorter dephasing component will dominate the overall line width, as already established by a similar calculation with SWCNTs.[37] The line widths, Γ, presented in the table are calculated using the formula

$$\Gamma = \frac{\hbar}{T_2^*} \tag{7}$$

where the pure-dephasing time $T_2^* = \tau_e$ is taken from the fit (5) for the ideal GNR and $T_2^* = [B\tau_e + (1 - B)\tau_g]/2$ is taken from the fit (6) for the GNRs with defects.

Comparison between the cumulant and direct calculations allows one to evaluate the extent of anharmonicity in the phonon motions that induce the dephasing. Generally, the two approaches agree in all cases. The agreement is best for

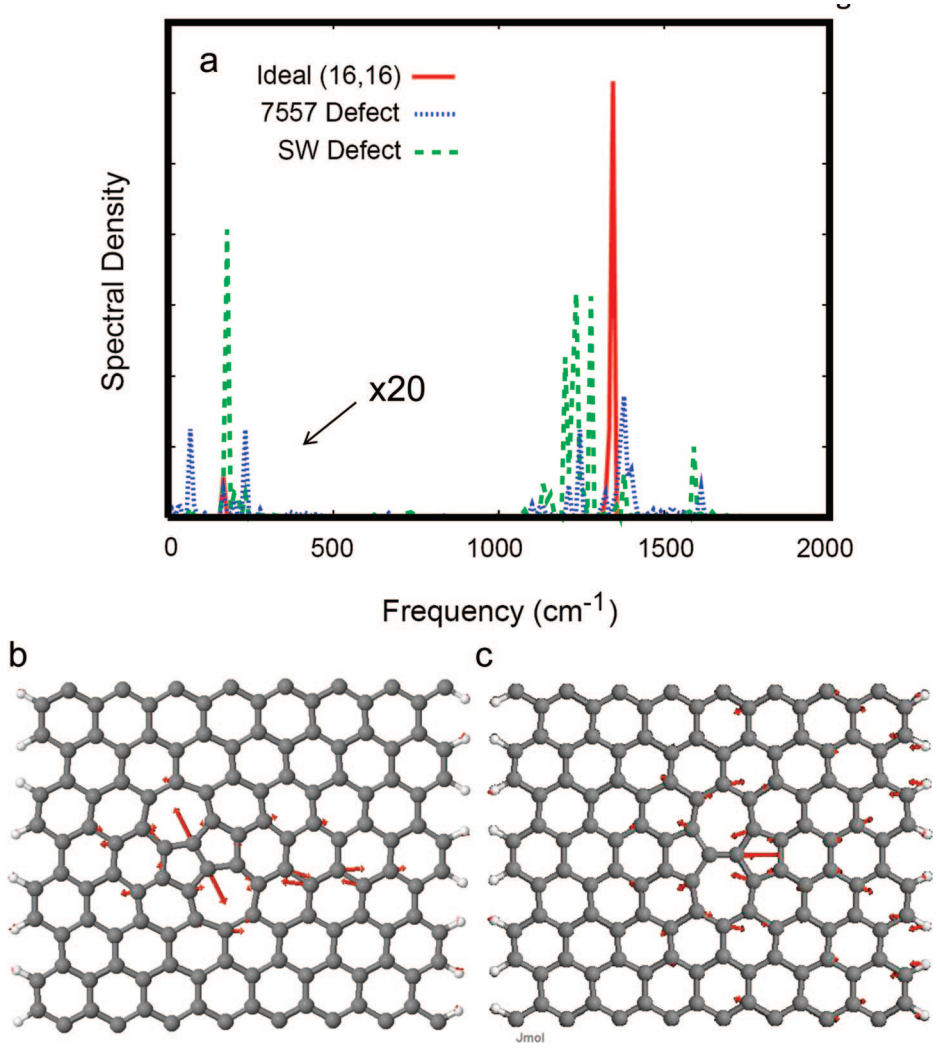

Figure 4. (a) Fourier transforms (FTs) of the autocorrelation functions shown in Figure 3. The FT intensities for the GNRs with defects were multiplied by 20 relative to that for the ideal GNR. (b and c) Typical normal modes associated with the 7557 and SW defects.

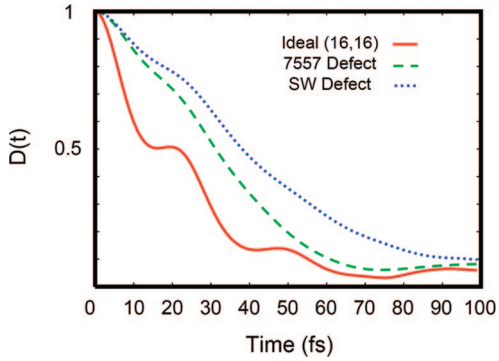

Figure 5. Pure-dephasing functions for the studied GNRs. The dephasing occurs faster for the ideal (16,16) ribbon due to stronger electron−phonon coupling.

the 7557 defect; see Table 1. The defect creates well localized electronic states, Figure 2, and phonon modes, Figure 4, which are quite harmonic. The deviations between the cumulant and direct data are greater for the ideal GNR and the SW defect. The phonon modes are more anharmonic in these cases, since they extend to the flexible GNR edges. The lack of rigidity inherent in the 2D plane of graphene

Table 1. Pure-Dephasing Times T_2* and Corresponding Homogeneous Line Widths Γ, Equation 3, Obtained by Fitting the Cumulant 3 and Direct 4 Dephasing Functions to Equations 5 and 6, Respectively[a]

ribbon	τ (fs)	ω (fs $^{-1}$)	A	Γ (meV)
(16,16)	23.5/25.8	0.259/0.257	0.024/0.069	28.0/25.5
defect	τ_e (fs)	τ_g (fs)	B	Γ (meV)
7557	41.8/48.9	39.9/35.7	0.38/0.30	16.1/16.5
SW	69.8/57.3	42.3/46.0	0.54/0.44	11.5/12.9

[a] The first/second number in each cell corresponds to the cumulant/direct calculation.

creates further anharmonicity. Recent investigations into the structure of the atomic layer of graphene showed ripples in the 2D lattice, causing deviations from the perfect 2D structure and stabilizing GNRs.[3]

Both direct and cumulant schemes show that the defects slow down the dephasing process in GNRs. This surprising discovery is in stark contrast with SWCNTs, in which the 7557 and SW defects accelerate the dephasing.[37] As with SWCNTs, the defects induce a large amount of disorder into the phonon spectrum and allow for coupling to a larger range of modes, Figure 4. However, the electron−phonon coupling

is weaker with defects compared to the ideal ribbon. The average fluctuation of the excitation energy caused by the vibrational motions is larger in the ideal ribbon by a factor of 4, as indicated by the initial values of the ACFs shown in Figure 3. This difference in the fluctuation amplitude has a more profound effect on the dephasing function than the faster decay of the ACFs seen with the defects. Comparing the two defects between each other, we observe that the electron−phonon coupling is weaker with the SW defect and the dephasing is slower in this case. This corresponds very well to SWCNTs,[37] in which the stronger 7557 defect induces faster dephasing as well. In fact, the pure-dephasing times calculated for the SW defect in the GNR and SWCNT[37] are very similar. The pure-dephasing times calculated for the 7557 defect are different between the GNR and SWCNT. Due to its intrinsic flexibility, the GNR is able to accommodate the defect and relax its geometric strain much more easily than the SWCNT. As a result, the dephasing induced by the 7557 defect is slower in the GNR than in the SWCNT.

The line widths calculated on the basis of the dephasing times using eq 7 can be used experimentally to establish the presence of defects. The calculation predicts that the optical lines should be broader in the ideal GNRs than in the GNR with the defects. The difference in the line width is about a factor of 2 for the current GNRs. The situation is reversed from the SWCNT case, in which defect can be detected by broader, rather than by narrower optical bands.[37,42] The optical bands of ideal GNRs are broader than the bands of the ideal SWCNTs, because GNRs are less rigid than SWCNTs and allow for stronger electron−phonon coupling.

In conclusion, for the first time, we have applied ab initio molecular dynamics in order to investigate the phonon-induced dephasing and line widths of the lowest energy electronic excitations in a narrow GNR with and without defects. The method was tested previously with similar size SWCNTs[37] as well as quantum dots[43] and gave excellent agreement with the experimental data. Compared to the perfect nanotubes, the dephasing in the perfect nanoribbon is a factor of 2 faster. The dephasing time depends on the amplitude of the atomic motion. The rigidity of SWCNTs restricts the extent of the atomic motion, resulting in slower dephasing. The homogeneous optical line width associated with the pure-dephasing process is twice larger in the GNR than that in SWCNTs. The dephasing in the ideal ribbon is induced primarily by the disorder mode seen in bulk graphite.

The reported calculations have been performed on isolated GNRs, most closely corresponding to GNRs grown across nanostructures[21] or etched substrates.[22] GNRs supported by substrates[4] or synthesized in solution[5] may exhibit different dephasing times and optical line widths, much as carbon nanotubes in solution or polymer matrices[44] have broader optical line widths than nanotubes suspended in air.[21] It is not clear in present, however, whether a substrate will accelerate or decelerate the dephasing. The dephasing may become faster due to the presence of new interactions. At the same time, the substrate can make the ribbon stiffer, reducing the extent of atomic motion and slowing down the dephasing.

In contrast to the nanotubes, defects in the nanoribbon slow down the dephasing. The dephasing induced by the bond-rotation defect is very similar in both GNR and SWCNT. The bond-insertion defect behaves differently in the two materials, because the nanoribbon can relax the strain induced by the defect, while the defect remains strained in the nanotube. The fact that the electron−phonon interaction induced by the defects is weaker than the interaction in the ideal GNR has very important practical implications. In particular, it ensures that the problem of defect-induced fluorescence quenching and energy dissipation, which limits many applications of semiconducting SWCNTs, should not arise with GNRs.

Acknowledgment. The research was supported by grants from NSF CHE-0701517, IGERT, and ACS-PRF 46772-AC6.

References

(1) Kroto, H. W.; Heath, J. R.; O'Brien, S. C.; Curl, R. F.; Smalley, R. E. *Nature* **1985**, *318*, 162.
(2) Iijima, S. *Nature* **1991**, *354*, 56.
(3) Novoselov, K. S.; Geim, A. K.; Morozov, S. V.; Jiang, D.; Zhang, Y.; Dubonos, S. V.; Grigorieva, I. V.; Firsov, A. A. *Science* **2004**, *306*, 666.
(4) Coraux, J.; N'Diaye, A. T.; Busse, C.; Michely, T. *Nano Lett.* **2008**, *8*, 565.
(5) Li, X.; Wang, X.; Zhang, L.; Lee, S.; Dai, H. *Science* **2008**, *319*, 1229.
(6) Avouris, P.; Chen, Z. H.; Perebeinos, V. *Nat. Nanotechnol.* **2007**, *2*, 605.
(7) Avouris, P.; Freitag, M.; Perebeinos, V. *Carbon Nanotubes* **2008**, *111*, 423.
(8) Barone, V.; Hod, O.; Scuseria, G. E. *Nano Lett.* **2006**, *6*, 2748.
(9) Yang, L.; Park, C. H.; Son, Y. W.; Cohen, M. L.; Louie, S. G. *Phys. Rev. Lett.* **2007**, *99*, 186801.
(10) Son, Y. W.; Cohen, M. L.; Louie, S. G. *Nature* **2006**, *444*, 347.
(11) Ponomarenko, L. A.; Schedin, F.; Katsnelson, M. I.; Yang, R.; Hill, E. W.; Novoselov, K. S.; Geim, A. K. *Science* **2008**, *320*, 356.
(12) Chen, Z.; Lin, Y. M.; Rooks, M. J.; Avouris, P. *Physica E* **2007**, *40*, 228.
(13) Han, M. Y.; Ozyilmaz, B.; Zhang, Y. B.; Kim, P. *Phys. Rev. Lett.* **2007**, *98*, 206805.
(14) Hueso, L. E.; Pruneda, J. M.; Ferrari, V.; Burnell, G.; Valdes-Herrera, J. P.; Simons, B. D.; Littlewood, P. B.; Artacho, E.; Fert, A.; Mathur, N. D. *Nature* **2007**, *445*, 410.
(15) Hod, O.; Barone, V.; Scuseria, G. E. *Phys. Rev. B* **2008**, *77*, 035411.
(16) Jarillo-Herrero, P.; van Dam, J. A.; Kouwenhoven, L. P. *Nature* **2006**, *439*, 953.
(17) Mukamel, S. *Principles of Nonlinear Optical Spectroscopy*; Oxford University Press: New York, 1995.
(18) Carlson, L. J.; Krauss, T. D. *Acc. Chem. Res.* **2008**, *41*, 235.
(19) Htoon, H.; O'Connell, M. J.; Doorn, S. K.; Klimov, V. I. *Phys. Rev. Lett.* **2005**, *94*, 127403.
(20) Jorio, A.; Dresselhaus, G.; Dresselhaus, M. S. *Carbon Nanotubes* Springer: Berlin, 2008.
(21) Lefebvre, J.; Finnie, P.; Homma, Y. *Phys. Rev. B* **2004**, *70*, 045419.
(22) Lee, J. U. *Appl. Phys. Lett.* **2005**, *87*, 073101.
(23) Sternberg, M.; Curtiss, L. A.; Gruen, D. M.; Kedziora, G.; Horner, D. A.; Redfern, P. C.; Zapol, P. *Phys. Rev. Lett.* **2006**, *96*, 075506.
(24) Horner, D. A.; Redfern, P. C.; Sternberg, M.; Zapol, P.; Curtiss, L. A. *Chem. Phys. Lett.* **2007**, *450*, 71.
(25) Kresse, G.; Furthmüller, J. *Comput. Mater. Sci.* **1996**, *6*, 15.
(26) Perdew, J. P. *Electronic Structure of Solids*; Akademie Verlag: Berlin, 1991.
(27) Blochl, P. E. *Phys. Rev. B* **1994**, *50*, 17953.
(28) Kresse, G.; Joubert, D. *Phys. Rev. B* **1999**, *59*, 1758.
(29) Butscher, S.; Milde, F.; Hirtschulz, M.; Malic, E.; Knorr, A. *Appl. Phys. Lett.* **2007**, *91*, 203103.

(30) Kampfrath, T.; Perfetti, L.; Schapper, F.; Frischkorn, C.; Wolf, M. *Phys. Rev. Lett.* **2005**, *95*, 187403.
(31) Habenicht, B. F.; Craig, C. F.; Prezhdo, O. V. *Phys. Rev. Lett.* **2006**, *96*, 187401.
(32) Huang, L.; Pedrosa, H. N.; Krauss, T. D. *Phys. Rev. Lett.* **2004**, *93*, 017403.
(33) Skinner, J. L. *Annu. Rev. Phys. Chem.* **1988**, *39*, 463.
(34) Ferrari, A. C.; Meyer, J. C.; Scaradaci, V.; Casiraghi, C.; Lazzeri, M.; Mauri, F.; Piscanec, S.; Jiang, D.; Novoselov, K. S.; Roth, S.; Geim, A. K. *Phys. Rev. Lett.* **2006**, *97*, 187401.
(35) Habenicht, B. F.; Prezhdo, O. V. *Phys. Rev. Lett.* **2008**, *100*, 197402.
(36) Perebinos, V.; Tersoff, J.; Avouris, P. *Phys. Rev. Lett.* **2005**, *94*, 086802.
(37) Habenicht, B. F.; Kamisaka, H.; Yamashita, K.; Prezhdo, O. V. *Nano Lett.* **2007**, *7*, 3260. The *y*-axis units in Figure 2 should read "atomic units".
(38) Kilina, S.; Tretiak, S. *Adv. Funct. Mater.* **2007**, *17*, 3405.
(39) Tretiak, S.; Kilina, S.; Piratinski, A.; Saxena, A.; Martin, R. L.; Bishop, A. R. *Nano Lett.* **2007**, *7*, 86.
(40) Schwartz, B. J. *Annu. Rev. Phys. Chem.* **2003**, *54*, 141.
(41) Martini, I. B.; Smith, A. D.; Schwartz, B. J. *Phys. Rev. B* **2004**, *69*, 035204.
(42) Gokus, T.; Hartschuh, A.; Harutyunyan, H.; Allegrini, M.; Hennrich, F.; Kappes, M.; Green, A. A.; Hersam, M. C.; Araujo, P. T.; Jorio, A. *Appl. Phys. Lett.* **2008**, *92*, 153116.
(43) Kamisaka, H.; Kilina, S. V.; Yamashita, K.; Prezhdo, O. V. *Nano Lett.* **2006**, *6*, 2295.
(44) O'Connell, M. J. *Science* **2002**, *297*, 787.

NL801556N